Time to lysis determines phage sensitivity to a cytidine deaminase toxin/antitoxin bacterial defense system

Brian Y. Hsueh[1@], Ram Sanath-Kumar[1], Amber M. Bedore[1], and Christopher M. Waters[1*]

[1]Department of Microbiology and Molecular Genetics, Michigan State University, East Lansing, Michigan, USA, 48824

Running Title: Lysis timing determines AvcID Toxin-Antitoxin sensitivity

[@]Current address: Meso Scale Diagnostics LLC, Rockville, Maryland, USA 20850

[*]**Corresponding Author:**

5180 Biomedical and Physical Sciences

567 Wilson Road

East Lansing, MI 48824

Telephone 517-884-5360

E-mail: watersc3@msu.edu

Keywords: cytidine deaminase, toxin-antitoxin, phage, antiphage defense, transcriptional shutoff

Abbreviations:

CBASS	Cyclic oligonucleotide-based antiphage signaling systems
CFU	Colony forming units
dCMP	Deoxycytidine monophosphate
dCTP	Deoxycytidine triphosphate
dUMP	Deoxyuridine monophosphate

dUTP	Deoxyuridine triphosphate
ETEC	Enterotoxigenic *E. coli*
MGE	Mobile genetic element
MOI	Multiplicity of infection
PFU	Plaque forming units
RM	Restriction/Modification
TA	Toxin-antitoxin
TEM	Transmission Electron Microscopy
WT	Wild type

ABSTRACT

Toxin-antitoxin (TA) systems are ubiquitous two-gene loci that bacteria use to regulate cellular processes such as phage defense. Here, we demonstrate the mechanism by which a novel type III TA system, *avcID*, is activated and confers resistance to phage infection. The toxin of the system (AvcD) is a deoxycytidylate deaminase that converts deoxycytidines (dC) to dexoyuridines (dU), while the RNA antitoxin (AvcI) inhibits AvcD activity. We have shown that AvcD deaminated dC nucleotides upon phage infection, but the molecular mechanism that activated AvcD was unknown. Here we show that the activation of AvcD arises from phage-induced shutoff of host transcription, leading to degradation of the labile AvcI. AvcD activation and nucleotide depletion not only decreases phage replication but also increases the formation of defective phage virions. Surprisingly, infection of phages such as T7 that are not inhibited by AvcID also lead to AvcI RNA antitoxin degradation and AvcD activation, suggesting that depletion of AvcI is not sufficient to confer protection against some phage. Rather, our results support that phage with a longer lysis time like T5 are sensitive to AvcID-mediated protection while those with a shorter lysis time like T7 are resistant.

AUTHOR'S SUMMARY

Numerous diverse antiphage defense systems have been discovered in the past several years, but the mechanisms of how these systems are activated upon phage infection and why these systems protect against some phage but not others are poorly understood. The AvcID toxin-antitoxin phage defense system depletes nucleotides of the dC pool inside the host upon phage infection. We show that phage inhibition of host cell transcription activates this system by depleting the AvcI inhibitory sRNA, which inhibits production of phage and leads to the formation of defective virions. Additionally, we determined that phage lysis time is a key factor that influences sensitivity to AvcID with faster replicating phage exhibiting resistance to its

effects. This study has implications for understanding the factors that influence bacterial host/phage dynamics.

INTRODUCTION

Bacteria must respond and adapt to a plethora of different challenges in order to survive and propagate. One such challenge is predatory bacteriophage (phage). To counter phage infection, bacteria have evolved a diverse repertoire of molecular phage defense mechanisms including Restriction/Modification (RMs), CRISPR/Cas, cyclic-oligonucleotide-based antiphage systems (CBASS), retrons, and toxin-antitoxin (TA) systems [1–7]. TA systems were first discovered on plasmids (*e.g.* Type I) and later were ubiquitously found on bacterial and phage chromosomes [8–10]. These modules typically constitute a two-gene operon that encodes diverse toxins along with a peptide or RNA antitoxin that neutralizes the toxin [11–13]. There are currently eight classes (I-VIII) of TA systems based on the nature of the antitoxin and the mechanism by which it regulates the toxin [11, 13]. The toxins are generally proteins with the exception of the type VIII system, in which the toxin is a small RNA (sRNA) [13, 14]. In the case of type I, III, and VIII TA systems, the antitoxins are sRNAs while the rest of the classes have small peptide antitoxins [13]. Antitoxins are more abundant than their cognate toxins but are more labile, freeing the toxins to exert their growth-inhibition functions when expression of both genes is inhibited [15].

Though many past studies employed abiotic stressors (*i.e.* antibiotics, oxidative agents), to test the induction of type II TA systems, recent findings show that biotic stress, such as phage infection, can also activate TA systems [13, 16]. RMs encoded in Type I TA systems inhibit phage infections and promote plasmid maintenance [2, 8]. Similarly, type I-IV TA systems have demonstrated that one of their primary physiological roles is to limit phage infections [17–20]. Additionally, TA modules are not only clustered and closely connected to mobile genetic

elements (MGEs), but they also mediate the stabilization of MGEs by limiting gene reduction [21]. They also are highly abundant in free-living bacteria but not symbiotic, host-associated species [22], supporting that MGEs are evolutionarily beneficial and important in bacteria that are constantly challenged by phages.

AvcID is a newly discovered, broadly conserved Type III TA system that encodes the AvcD toxin and AvcI antitoxin. AvcD is a deoxyctidine (dU) deaminase that deaminates dCTP and dCMP nucleotides to dUTP and dUMP, respectively, leading to a disruption in nucleotide metabolism after phage infection [23, 24]. AvcI is a noncoding RNA that binds to and directly inhibits the activity of AvcD; however, the mechanism by which phage induce activity of the AvcID system remains unknown. Moreover, why AvcID inhibits infection of some phage while others are resistant to its activity is not understood. Here, we demonstrate that upon phage infection, the AvcI sRNA antitoxin is rapidly lost, allowing AvcD to deaminate dC pools. This activation leads to less phage production and the production of defective phage virions. Contrary to our hypothesis, phage resistant to AvcID-mediated protection still depleted AvcI and activated AvcD upon infection, suggesting other dynamics of phage/host interactions are important for sensitivity to AvcD. Our results suggest that the lysis time, or the time it takes from phage infection to cell lysis is a key factor mediating sensitivity to AvcID as phage with rapid lysis times are resistant to AvcID-mediated protection.

RESULTS

AvcID provides phage defense in liquid cultures

Previous studies demonstrated that AvcID systems derived from *Vibrio cholerae, V. parahaemolyticus, and Escherichia coli* ETEC can reduce the dC nucleotide pool upon phage infection, yet their respective resistance profiles as measured by efficiency of plaquing (EOP) assays are different [23, 24]. For instance, *V. parahaemolyticus* AvcID provided protection against T3, T5, T6, and SECΦ18 phages whereas *E. coli* ETEC AvcID provided protection

against T3, SECΦ17, SECΦ18, and SECΦ27 [23]. To better understand the activation of AvcID systems and the molecular mechanisms underlying phage defense specificity, we studied the AvcID system derived from *V. parahaemolyticus* in a heterologous *E. coli* host as it provides robust protection against well-characterized T-type coliphages, such as T5. For the rest of this study, "AvcID" refers to the *V. parahaemolyticus avcID* we previously described [23].

Since the protection conferred by the AvcID system has thus far been based on comparing phage titers on agar plates [23], we wondered if the AvcID system could also confer protection in liquid culture as this would be a more robust experimental system to explore molecular mechanism. To answer this question, we generated *E. coli* cells harboring genes encoding for either the wild type AvcID (pAvcID) or the inactive AvcID$^{S49K+E376A}$ mutant enzyme (pAvcID*), expressed from their native promoters on a medium copy number plasmid. These *E. coli* strains were infected with either T5 or T7 at varying multiplicities of infection (MOI), and bacterial growth was tracked by measuring OD_{600} over time. The OD_{600} of T5 infected cultures harboring AvcID was higher throughout the experiment compared to cultures harboring AvcID* at all the MOIs tested, and at lower MOIs AvcID completely protected the culture from T5 (Fig. 1A). Alternatively, AvcID showed no protection against T7 infection in liquid culture at any MOI (Fig. 1B). These data show that AvcID provides *E. coli* with defense against T5 but not T7 in liquid culture.

AvcD is activated by transcriptional shutoff

AvcI and AvcD form a complex in vitro, and AvcD is inhibited by the sRNA AvcI, suggesting AvcD inhibition is linked to the assembly of the complex [23]. A common mechanism that lytic phage employ upon infection is inhibition of host cell transcription [19, 25–27]. Given that antitoxins are unstable, we hypothesized that AvcI is degraded upon inhibition of host cell transcription by infecting phage, leading to activation of AvcD. To test this, we assessed the stability of AvcI by Northern blot from *E. coli* cells encoding the *avcID* locus on a plasmid under

the expression of its native promoter. Likewise, to determine whether AvcD protein levels changed concurrently with changes in *avcI* RNA levels, we quantified the AvcD protein using a Western blot with antibodies specific to a C-terminal 6xHis tag. Notably, the full length of the *avcI* transcript is slightly smaller than the 300 ribonucleotide bases, which is longer than the minimum functional length of AvcI of ~171 bases that was previously determined (Fig. S1) [23]. The levels of AvcI rapidly decreased when cells were treated with the transcriptional inhibitor rifampicin, showing that in the absence of new transcription, AvcI is degraded (Fig. 2A). Importantly, spectinomycin, which inhibits protein synthesis instead of transcription, did not decrease *avcI* levels (Fig. 2B), indicating that the degradation was specific to transcriptional shutoff. These results are consistent with our previous study showing that rifampicin but not spectinomycin activated AvcD in *V. cholerae* [23].

We also infected these cells with phages T5 and T7 and quantified AvcI and AvcD over time (Fig. 2C-D). The half-life of the *avcI* transcript ranged from 1.5 min with T7 to 6.7 min with T5 (Fig. S2). The fact that AvcI is degraded faster during T7 compared with T5 is a surprising result given that AvcID provides protection against T5 phage but not T7. Concurrently, we also found that AvcD protein levels did not change significantly in any of the conditions tested (Fig. 2A-D). To determine whether AvcD is activated upon loss of AvcI, we measured the intracellular abundance of dCTP and dCMP using UPLC-MS/MS before and after infecting the cells containing active or inactive *avcID* with T5 or T7 phages. Surprisingly, both T5 and T7 infections significantly decreased intracellular dCTP and dCMP in cells containing active *avcID*, demonstrating that both phages activate AvcD (Figs. 3A-B). We also noted that T5 decreases intracellular dCMP in cells containing inactive *avcID* (Fig. 3B). We hypothesize this result is due to a T5 encoded 5' monophosphatase (*dmp*) which participates in the final stages of host DNA degradation by dephosphorylating 5'-dNMP's substrates [28]. Collectively, these results suggest that transcriptional shutoff coupled with the instability of the *avcI* RNA leads to the release of

existing AvcD from inhibition upon both T5 and T7 phage infection, but activation of AvcD is not sufficient to protect against T7 phage infection.

AvcID drives production of defective T5 phage

We found that AvcID provides resistance to T5 but not T7 (Figs. 1A-B), yet both phages induce the degradation of AvcI and the activation of AvcD deamination (Figs. 2-3). To further understand this difference, we quantified the production of phage and the viability of *E. coli* hosts during liquid T5 and T7 phage infection assays for *E. coli* carrying either AvcID or inactive AvcID*. Infected *E. coli* cells were separated from the phage lysates by centrifugation to measure colony forming units (CFUs) and plaque forming units (PFUs). Cells harboring AvcID infected with T5 had more viable CFUs than cells harboring inactive AvcID* after two hours of infection (Fig. 4A). Furthermore, the AvcID-containing population generated ~100-fold fewer PFUs than AvcID*-containing cells (Fig. 4B), supporting the notion that AvcID inhibits the accumulation of functional T5 phages. Consistent with our liquid infection results described above, AvcID did not impact the number of CFUs and PFUs when cells were infected with T7 (Figs. 4D-E).

Since a plaque assay only quantifies viable phages, we speculated that the total viral particles produced could be underestimated if some of those virions were non-viable. To determine total virions produced, we quantified the abundance of a specific phage gene for T5 and T7 in the phage particle samples using qPCR. Importantly, these samples had been treated with DNase ensuring that only genomes protected by phage virions were quantified by this assay. Our results indicated that the total number of T5 phage genomes decreased over time in infected cultures of AvcID-containing cells compared to AvcID*-containing cells. However, the magnitude of this decrease was less than that observed for the difference in PFUs between the two samples (Fig. 4B, C). For example, at the two-hour time point, there was a difference of ~100-fold in PFUs but only a difference of 20-fold in virions measured with qPCR. We observed

no significant difference in genome abundance between AvcID and AvcID* encoding cultures when infected with T7 (Fig. 4F).

The greater magnitude difference for T5 of PFUs compared to phage genomes suggested that the majority of virions produced from AvcID-containing cells contained genomes that were defective to infect new cells and form plaques. We calculated the percentage of viable phages by quantifying the ratio between PFUs and genome abundance of AvcID or AvcID* infected cultures. Using this analysis, we estimated that by 30 min only 30% of T5 phage derived from cells containing AvcID were functional, and the proportion of functional phage generally decreased over time, suggesting that AvcID drives formation of defective T5 phage virions (Fig. 4G). In contrast, a similar analysis for T7 indicates that nearly all the T7 phages were viable even when they were from cells encoding *avcID* (Fig. 4G). This indicates that AvcID confers protection by both decreasing phage replication and increasing defective phage production for T5 while T7 can overcome these negative effects of AvcID through an unknown mechanism.

Consistent with our observation that defective T5 phage are generated from *avcID*-encoding cells, transmission electron microscopy (TEM) images of negatively stained samples revealed that particles produced from cells containing active AvcID have more defective phage capsids—*i.e.* broken particles, or capsids with aberrant morphology, containing no genome and without attached tails (Fig. 5A), compared to T5 phage from cells containing AvcID* (Fig. 5B). Images of negatively stained particles of T7 isolated from *avcID* encoding cells showed no such defects and the virions looked normal (Fig 5C). Together, the TEM results corroborate our previous experiments confirming that the AvcID system inhibits production of functional T5 phage particles.

Ung and Dut do not contribute to AvcID antiphage defense

We have previously demonstrated that AvcD can deaminate dCTP to dUTP. Increased dUTP concentrations in cells may lead to an increased frequency of dUMP being incorporated into the phage genomic DNA in place of dTMP by DNA polymerases during replication. Incorporated dUMP in genomic DNA can be targeted by the DNA repair enzyme uracil-N-glycosylate (Ung), leading to formation of an abasic site that could block DNA replication. Moreover, an apurinic or apyrimidinic endonuclease can then cleave the DNA at the abasic site, resulting in a nicked DNA strand [29, 30]. We hypothesized that the decreased viability of phage produced in AvcID expressing cells could be due to incorporation of uracils in the genomic DNA of T5 and excessive repair by Ung upon infection of new hosts. To determine whether AvcD and Ung function together to reduce phage infection, we infected *E. coli* MG1655 or Δ*ung E. coli* NR8052 encoding *avcID* or *avcID** with T5 phage, measured the relative phage titer, and further tracked bacterial growth by OD_{600} over time. We hypothesized that the Δ*ung* mutant would not exhibit as robust of protection from T5 as the WT *E. coli.* Contrary to our hypothesis, the OD_{600} of both strain backgrounds carrying active AvcID exhibited similar protection, suggesting that Ung is not required for AvcID to protect *E. coli* from T5 phage (Fig. 6A). When comparing relative phage titer, we observed no difference in AvcID-mediated protection from T5 in the presence or absence of *ung* (Fig. 6B). Finally, we infected *E. coli* MG1655 containing either AvcID or AvcID* with T5 phage while overexpressing a dUTPase (*dut*) to reduce accumulation of dUTP, thereby preventing potential incorporation of uracil into phage genomes. The overexpression of Dut had no effect on the phage defense conferred by AvcID (Fig. 6C). Together, these data suggest that accumulation of dUTP or incorporation of uracils into the phage genome does not contribute to AvcID-mediated protection.

T7 mutants with delayed lysis time are susceptible to AvcID

Our results demonstrated that both T5 and T7 activate AvcID, but this system only protects against T5 infection. When considering this discrepancy, we noted that T7 has a much

faster lysis time compared to T5 (~22.5 min vs. 60 min), suggesting a model in which T7 could replicate enough genomes before AvcID is activated to mitigate its protective effects. To test if lysis time is a key factor in AvcID-sensitivity, we mutagenized T7 phage *in vitro* with the alkylating agent methyl methanesulfonate (MMS). This treatment increases the lysis time for the first cycle of phage infection by creating lesions in the DNA that must first be repaired by the host DNA repair machinery before replication can be initiated [31]. At a MOI of 0.1, AvcID showed poor protection against untreated T7 and MMS-treated T7 (Figs. S3A-B). However, at a MOI of 0.0001, AvcID delayed the complete lysis of the population by MMS-treated T7 phage (Figs. S3C-D). Ultimately, however, the rate of the population drop was identical in all conditions. We interpret this result to mean that after a delay in the lysis of the initial MMS-treated T7, AvcID was unable to protect against subsequent rounds of phage infection.

To further explore the impact of lysis time on AvcID-mediated protection, we infected *E. coli* carrying AvcID or AvcID* with the T7 mutant phage $T7^{412}$ (gift of Ian Molineux) that has a delayed lysis time of 40 min (see materials and methods for the specific mutations of this phage). Unlike WT T7, the plaque formation of the $T7^{412}$ mutant phage was completely inhibited by *avcID* (Figs. 7A-B). We next quantified the viability of hosts, production of functional phage, and total phage genome abundance with qPCR of $T7^{412}$ in AvcID and AvcID* encoding cells. Cells containing AvcID infected with $T7^{412}$ had more viable CFUs than cells carrying AvcID* (Fig. 7C), and the AvcID-containing cells had up to ~5 orders of magnitude less $T7^{412}$ PFUs than AvcID*-containing cells (Fig. 7D). Additionally, the total number of $T7^{412}$ genomes quantified using qPCR decreased over time in infected cultures of AvcID-containing cells compared to the inactive variant (Fig. 7E). Using these results, we estimated the proportion of functional $T7^{412}$ by 30 min was only approximately 2% of the total phage virions (Fig. 7F). These data indicate that AvcID confers protection against $T7^{412}$ by increasing defective phage production and generating non-functional phage, similar to our results for T5.

Relationship between phage replication time and AvcID protection

Our results suggested that lysis time is a key factor that determines phage sensitivity or resistance to AvcID. To further explore this idea, we measured the association between phage lysis time and the amount of protection conferred by AvcID in liquid cultures. We define the phage lysis time as the point in which a liquid culture begins to decrease in OD_{600} during phage infection at a MOI of 1. The amount of protection conferred by AvcID was determined by the difference in the area under the growth curve between the cells encoding either *avcID* or *avcID** at a MOI of 0.01 (Figs. 1, S4). Our results show that in liquid growth conditions, we see strong protection conferred by AvcID against T5 and SECΦ18 phages (Figs. 1, 8, S3). These two phages have two of the longest lysis times at over 60 minutes, with only T4 having a longer lysis time of 75 min (Fig. 8). However, AvcID did not protect *E. coli* from infection by phage with shorter lysis times. We found no clear relationship between the phage genome size and their respective lysis time (Fig. S5). Together these results suggest that lysis time, but not genome size, contributes to phage sensitivity to AvcID.

DISCUSSION

Phage predation is a constant evolutionary pressure that shapes the diversity and fitness of bacteria that has driven the evolution of multiple antiphage defense systems. The underlying mechanisms of certain antiphage defenses such as RMs, which utilize DNA modifications to distinguish host and foreign DNA, are well-characterized [2, 32, 33]. On the contrary, the mechanism of activation of the cyclic nucleotide-based systems (*i.e.,* CBASS) in response to phage infection is generally not understood [3, 34]. Moreover, although many novel phage defense systems have been recently identified, it is typically unclear why they provide protection against some phage but not others [7, 23, 24, 35, 36]. Here, we reveal the mechanism of how the AvcID TA system is activated in response to phage infection and its impact on the phage's morphogenetic pathway. We also determined that lysis time is an important factor that drives

AvcID to specifically protect against longer replicating phage like T5 while it is ineffective against faster replicating phage like T7.

Cessation of transcription is a hallmark of infection by many phages [27, 28, 37]. Our results demonstrate that transcriptional shutoff leads to the degradation of AvcI, releasing AvcD to deaminate dC nucleotides. This mode of activation is consistent with other TA systems, such as the ToxIN system [19, 38] and previous work showing that inhibition of transcription activates AvcD, although the mechanism for this activation was not known [23, 24] . This work is the first to show that this activation is due to degradation of the AvcI sRNA antitoxin. The AvcI antitoxin is produced at high abundance compared to AvcD [23]. In other TA systems, there is typically a Rho-independent terminator located between the toxin and antitoxin genes [39, 40]. However, sequence analysis did not predict such a terminator between *avcI* and *avcD,* and thus how the AvcI sRNA is formed and produced at much higher levels than AvcD requires further study.

Though AvcID did not provide protection against T7, *avcI* transcripts were rapidly degraded upon T7 infection, implying that *avcI* levels decrease when cells undergo transcriptional inhibition regardless of the cause. However, the activation of AvcD does not have any detrimental effect on the viability of T7, in contrast to T5, implying that T7 has evolved to disregard any detrimental effects inflicted by AvcID or similar phage defense systems. Given that we observed no difference in viable phage from functional AvcID versus AvcID* containing cells (Fig. 4), we suggest that even in the presence of AvcID and depleted dCTP, T7 replicates enough genomes to fully package all the capsid heads that are produced. Phage can synthesize more genomes than capsid heads, consistent with this interpretation [41, 42]. It should be noted that examination of AvcD orthologs from *E. coli* expressed in a heterologous *E. coli* host did show protection against T7 using a plaquing assay [24]. This result highlights the high degree of specificity in phage protection for each defense system. The reason for this difference between these studies is not clear, but we speculate it may be due to the specific molecular features of the two AvcD systems being studied or differences in the T7 phage that were tested.

Our analysis of population dynamics of T5 infected cultures suggested that AvcID not only impacts overall synthesis of T5 genomes, but it also leads to the formation of non-viable phage capsids. This conclusion is supported by TEM images that reveal most of the T5 phages are defective when AvcD is active. The depletion of dCTP and dCMP could have downstream impacts on the timing of DNA packaging or stability of phage virions, thus accounting for the reduced number of functional phages. The mechanism by which AvcID generates non-viable phage capsids is under investigation.

The growth of several well-known phages is inhibited when their DNA contains dUMP and Ung is present in the host cells. For example, to counter this negative effect T5 encodes its own dUTPase for reducing the dUTP level such that dUMP is limited in its genome [43] . However, the presence of the AvcID system prevents this T5 infection even in the absence of Ung, indicating that dUMP incorporation into the phage genome may not be the cause for the phage viability defect. Rather, our evidence suggests it is the depletion of the dC pool that is responsible for the reduction in functionality of T5 phage particles. Remarkably, the depletion in the dC pool has no effect on T7 viability even though its G/C content is approximately 52% [44]. T7 phage degrade the host genome and incorporate it into its own genome [45], which may partly offset the decreased dCTP nucleotide pool.

While we observed a relationship between the phage lysis time and resistance to AvcID, T4 has the longest infection time cycle, and it is not susceptible to AvcID defense (Figures S3E-F) [23]. Therefore, lysis time is not the sole factor mediating resistance to AvcID. The resistance of T4 might also be due to competition for dC nucleotides since T-even phages are known to possess enzymes that can methylate deoxycytosine-containing bases to evade bacterial RMs [46]. Whether this is also a strategy to resist AvcID is under investigation.

We obtained two lines of evidence that linked phage lysis time to AvcID sensitivity. First, treatment of phage virions with MMS, which is known to delay lysis time [31], enhanced sensitivity to AvcID (Fig. S2). Secondly, the resistance of T7 to AvcID can be completely

inhibited by altering its lysis time, as $T7^{412}$ had a slower lysis time and was completely susceptible to AvcID, even though this phage was fully capable of infecting and eradicating a non-AvcID expressing population [47]. This phage has a deletion of genes 0.5-1 with gene 1, the T7 RNA polymerase, inserted downstream of gene 12. The net result of these mutations is a delay in the synthesis of phage proteins and genome replication, increasing the time to lysis. The sensitivity of $T7^{412}$ suggests that the rapid lysis time of $T7^{WT}$ enables it to outrun the AvcID system to produce new virions before AvcID has completely depleted dC pools. A third line of evidence supporting the importance of lysis time in resistance to AvcID was illustrated in a recent study of a *V. cholerae* ICP3 phage, named M1Φ, that was partially restricted by the native *avcID* locus [48]. In this study, an AvcID-resistant mutant M2Φ was isolated, and strikingly the lysis time of this mutant (20 min) was twice as fast as the original phage (40 min) [48]. This result studying *avcID* in its native genome context and host is consistent with our conclusion that lysis time is an important driver of AvcID sensitivity and resistance [48].

Prior work on Type III TA systems suggests they are associated with abortive infections (Abi), which is defined as the host committing altruistic suicide to prevent phage replication [38]. However, overexpression of AvcD does not lead to cell death but does impair genome replication, and this effect can be rescued by inhibiting expression of the toxin or overexpressing *avcI* in trans [23]. Given that *avcI* is degraded, subsequently releasing existing AvcD to deaminate dC pools upon phage infection, we propose that protection conferred by AvcD is not through abortive infection. This conclusion is supported by our observation that infection of AvcID containing cells with a high MOI does not enhance killing of the host cells (Fig. 1).

Similar to the AvcID system, bacterial dGTPases protect against phage infection by dephosphorylating dGTP to dG to inhibit phage DNA replication and that this system is also activated upon phage-induced transcriptional shutoff [24]. It is, however, unclear whether the dGTPase system is a TA system. While other types of TA systems have been demonstrated to have antiphage properties, whether they are activated in a similar mechanism as the Type III

systems is unclear. Recently, the DarTG type II TA system was shown to provide phage defense by ADP-ribosylating phage DNA to disrupt DNA replication [36]. ParST, another type II TA system, exerts its effect via modification of cellular target Prs, which is involved in nucleotide biosynthesis, though the ParST system has not been demonstrated to be involved in phage defense. The mechanism of AvcID bears a resemblance to both DarTG and ParST but is distinct from both in terms of the mechanism for toxin function and activation. This suggests that manipulating nucleotide pools is a conserved function of many TA systems and antiphage defense mechanisms.

ACKNOWLEDGEMENTS

We thank Ry Young and Ian Molineux for their valuable suggestions and Ian Molineux for providing us with the T7 mutant phages. We thank Sundharraman Subramanian and Kristin Parent for the TEM imagining as well as the MSU RTSF Cryo-EM facility. We thank Keifei Yu for providing us with the NR8052 *E. coli* strain. We also thank MSU RTSF mass spectrometry facility core for their technical support. This work was supported by National Institutes of Health (NIH) grants GM139537 and AI158433 to C.M.W. Any opinions, findings, and conclusions or recommendations expressed in this material are those of the author(s) and do not necessarily reflect the views of the National Science Foundation.

MATERIALS AND METHODS

Bacterial Strains, Plasmids, and Growth Conditions

The strains, plasmids, and primers used in this study are listed in Supplemental Tables 1-3. Unless otherwise stated, cultures were grown in Luria-Bertani (LB) at 37°C and supplemented with ampicillin (100 µg/mL), kanamycin (100 µg/mL), and isopropyl-β-D-thiogalactoside (IPTG) (100 µg/mL) when needed. *E. coli* BW29427, a diaminopimelic acid

(DAP) auxotroph, was additionally supplemented with 300 µg/mL DAP. Plasmids were introduced into *E. coli* MG1655 or *E. coli* NR8052 through biparental conjugation using an *E. coli* BW29427 donor. P_{tac} inducible expression vectors were constructed by Gibson Assembly with inserts amplified by PCR and pEVS143 [49] each linearized by EcoRI and BamHI. Transformation of *E. coli* for ectopic expression experiments was performed using electroporation with DH10b for expression of pEVS143 derived plasmids.

Phage Propagation

Coliphages were propagated on *E. coli* MG1655 grown in LB, and their titer was determined using the small drop plaque assay method, as previously described [3, 50]. Briefly, 1 mL of overnight cultures were mixed with 50 mL of MMB agar (LB + 0.1 mM MnCl2 + 5 mM MgCl2 + 5 mM CaCl2 + 0.5% agar), tenfold serial dilutions of phages in MMB were spotted (5 µL) and incubated overnight at room temperature. The viral titer is expressed as plaque forming units per mL (pfu/mL).

Phage Infection in Liquid Culture

Overnight cultures of *E. coli* carrying the indicated AvcID plasmids were subcultured and grown to an OD_{600} of 0.3 and then mixed with phage at the indicated MOIs. A 150 µL aliquot of the mixtures were put into 96-well plates, and growth was measured at 2.5 min intervals with orbital shaking on a plate reader (SpectraMax M6) at 37°C for 8 hours. Data represents the mean ± SEM, n=3.

Plaque Assays and Imaging

E. coli MG1655 cells with indicated plasmids were grown in LB overnight at 37°C. Overnight cultures are subcultured 1:500 in melted MMB agar and solidified at room

438 temperature. Overnight cultures of *E. coli* MG1655 with inducible plasmids (pEV or
439 pDut) were subcultured 1:1000 in LB with 100 µM IPTG and grown until an OD_{600} of 1.0.
440 The cultures were then subcultured 1:500 in melted MMG agar supplemented with 100
441 µM IPTG and let to solidify at room temperature. Tenfold serial dilutions of coliphages in
442 MMB medium were spotted and incubated overnight at room temperature. We note that
443 in this assay, protection of AvcID was temperature dependent and lost at 37°C. This
444 temperature dependency is currently under investigation. The images of the plaques
445 were taken using ProteinSimple AlphaImager HP system.
446
447 **RNA Extraction for Northern Blot Following Phage Infection**
448 RNA isolation and qRT-PCR analysis were carried out as previously described [51].
449 Briefly, triplicate overnight cultures of *E. coli* carrying pAvcI-AvcD-6xHis were subcultured 1:100
450 in LB and grown to an OD_{600} of 0.3. 1 mL of each replicate was pelleted and flash-frozen by the
451 ethanol-dry ice slurry method. RNA was extracted using TRIzol® reagent following the
452 manufacturer's directions (Thermo Fischer Scientific™). RNA quality and quantity were
453 determined using a NanoDrop spectrophotometer (Thermo Fischer Scientific™).
454
455 **RNA Probe Synthesis and Purification**
456 The method for RNA probe production was modified from a previously described
457 protocol [23]. The AvcI DNA template for *in vitro* transcription was PCR amplified from pAvcI
458 using Q5 High-Fidelity DNA Polymerase (NEB™). To incorporate the T7 promoter into the final
459 AvcI DNA template, the forward primer included the T7 promoter sequence prior to the
460 homologous sequence for AvcI. Additionally, the first two residues of the reverse primer were 2′-
461 OMe modified to reduce 3′-end heterogeneity of the transcript [52]. The PCR reaction was
462 analyzed using a 1% agarose gel, and the band corresponding to the AvcI DNA template was

463 excised and gel purified using Promega Gel Extraction and PCR clean up kit. AvcI RNA was
464 synthesized by *in vitro* transcription using the T7-AvcI reverse complement DNA template and
465 the HiScribe™ T7 High Yield RNA Synthesis Kit (NEB™). Bio-11-UTP was included during the
466 transcription reaction for Northern blot detection purposes. The transcription reactions were
467 incubated at 37°C for 4 h. Following transcription, DNase I (NEB™) was added to a final
468 concentration of 1X per reaction and incubated at 37°C for an additional 15 min. AvcI was then
469 purified using Monarch® RNA Cleanup Kit (NEB™). Purity of the product was evaluated using a
470 1.0% TBE agarose gel. Individual aliquots of AvcI were flash-frozen using liquid nitrogen and
471 stored long-term at -80°C.
472
473 **Northern Blot Analysis Following Phage Infection and Half-life Quantification and**
474 **Analysis**
475 1.5-2 µg total RNA was diluted 1:1 in 2x sample buffer (Invitrogen™), loaded onto 7.5%
476 TBE-Urea PAGE gels, along with biotinylated sRNA ladder (Kerafast),and ran for 30 min or until
477 the front dye reached ~1 cm above the bottom of the gel at 200 V. RNA was then transferred to
478 BrightStar™-Plus Positively Charged Nylon Membrane (Invitrogen) with a Fisherbrand™
479 Semidry Blotting Apparatus (Fisher Scientific) and ran for 1 h at 250 mA. RNA was then
480 crosslinked to the membrane using the CX-2000 crosslinker compartment of the UVP
481 HybriLinker™ HL-2000 (Fisher Scientific™). Each side of the membrane was crosslinked at
482 1200 µjoules twice and dried at 50°C for at least 30 minutes to improve sensitivity. The
483 membranes were pre-hybridized for at least 60 minutes at 60°C in ULTRAhyb™ Ultrasensitive
484 Hybridization Buffer (Invitrogen™) with gentle shaking. Next, the pre-hybridization buffer was
485 removed, and hybridization buffer containing 1 nM of purified probe was added. The membrane
486 was hybridized for 12-16 hours at 60°C with gentle shaking. Next, the membrane was rinsed
487 twice every five minutes with 2x saline-sodium citrate (SSC) buffer, 0.1% SDS at 60°C and then
488 twice every 15 minutes with 0.1X SSC, 0.1% SDS at 60°C. The biotin-labeled probes were

detected using a Chemiluminescent Nucleic Acid Detection Module (Thermo Scientific™) at RT. The membranes were then imaged using the Amersham™ Imager 600. To determine the half-life of *avcI*, the band intensities were analyzed using the Fiji software and normalized to respective 0 min band intensity [53]. All Northern blots shown are representative of two independent biological replicates.

Western Blot Analysis of AvcD

Cells were collected in the same method as RNA extraction. Pellets were then resuspended at OD_{600} = 15 (~20 µL) in 2x Laemmi loading dye supplemented with 10% β-mercaptoethanol v/v, denatured for 10 min at 95°C, and centrifuged at 15k x g for 10 min. Samples were then analyzed by 4-20% SDS-PAGE gels (Mini-PROTEAN TGX Precast Protein Gels, Bio-Rad™) alongside size standards (Precision Protein Plus, Bio-Rad or PageRuler™ Plus Prestained Protein Ladder, Thermo Scientific™). Gels were run at room temperature for 60 min at 120 V in 1x Tris/glycine/SDS running buffer. Proteins were transferred to nitrocellulose membranes (Optitran™). The membranes were blocked using 5% skim milk and incubated with 1:5000 THE™ His Tag Antibody, mAb, Mouse (GenScript™) followed by 1:4000 Goat Anti-Mouse IgG Antibody (H&L) [HRP], pAb (GenScript™), treated with Pierce™ ECL Western Blotting Substrate, and imaged using an Amersham™ Imager 600. Western blots shown are representative of two independent biological replicates.

CFU/PFU Measurements Pre- and Post-Phage Infection

Overnight cultures were subcultured and split into two 10 mL aliquots and grown to an OD_{600} of ~0.3. One aliquot was mixed with phage (T5, MOI = 0.1; T7, MOI = 0.01; $T7^{412}$, MOI = 0.01) and the other with an equal volume of LB (uninfected control). Both were grown in a shaking incubator (210 rpm) at 37°C. At each indicated timepoint, 1.5 mL of culture was spun down. The supernatant from each tube was filter sterilized with 0.22 µM filter and transferred to

a new tube, and the cell pellets were washed twice with equal volume of LB to remove unadsorbed phage. For PFU measurements, the supernatants were serially diluted in MMB medium (LB + 0.1 mM MnCl2 + 5 mM MgCl2 + 5 mM CaCl2) and 5 µL of each dilution was spotted on a lawn of bacteria seeded in MMB agar plate (MMB + 0.5% agar). PFU plates were then grown at RT overnight and plaques quantified the following day. For CFU measurements, resuspended cell pellets were then incubated at 37°C for 5-10 minutes before being serially diluted 10-fold in PBS and 5 µL of each dilution was spotted on LB plates. CFU plates were then grown at 37°C overnight and colonies were quantified the following day.

UPLC-MS/MS dNTPS Quantification

Deoxynucleotide concentrations were determined as previously described [23] with minor modifications. Briefly, to measure the nucleotides after phage infection, cells were grown in LB overnight at 37°C. Overnight cultures were subcultured 1:100 in LB and grown to an OD_{600} of ~0.3. 3 mL of culture were collected for a time zero reading: 1.5 mL for dNTPs quantification and 1.5 mL for total protein quantification. The cultures were then infected with phage (T7, MOI of 5), and an additional 3 mL were removed at each indicated subsequent time point. Culture aliquots were collected by centrifugation at 15k x g for 1 min. Pellets were resuspended in 200 µL of chilled extraction buffer [acetonitrile, methanol, ultra-pure water, formic acid (2:2:1:0.02, v/v/v/v)]. To normalize in vivo nucleotide samples, the other 1.5 mL aliquot pellet was centrifuged at 15,000 x g for 1 min, resuspended in 200 µL lysis buffer F (20 mM Tris·HCl, 1% SDS, pH 6.8), and denatured for 10 min at 95°C. Denatured lysates were centrifuged at 15,000 x g for 1 min to pellet cellular debris, and the supernatant was used to quantify the total protein concentration in the sample by using the DC protein assay (Bio-Rad) and a BSA standard curve [54]. The concentrations of deoxynucleotides detected by UPLC-MS/MS were then normalized to total protein in each sample.

All samples resuspended in extraction buffer were immediately incubated at -20ºC for 30 min after collection and centrifuged at 15,000 x g for 1 min. The supernatant was transferred to a new tube, dried overnight in a speed vacuum, and finally resuspended in 100 µL ultra-pure water. Experimental samples and deoxynucleotides standards [1.9, 3.9, 7.8, 15.6, 31.3, 62.5, and 125 nM of dCTP (Invitrogen), dCMP (Sigma), dUTP (Sigma), and dUMP (Sigma)] were analyzed by UPLC-MS/MS using an Acquity Ultra Performance LC system (Waters) coupled with a Xevo TQ-S mass spectrometer (Waters) with an ESI source in negative ion mode.

Genomic Extraction and Quantification using qPCR

Phage genomes were extracted as previously described [55]. Briefly, phage lysates were treated with RNase A (Roche; 1 µg/mL), DNase I (NEB; 18 U), and lysozyme (Sigma-Aldrich; 1 mg/mL). Samples were incubated at 37ºC for 90 min, and then the DNase was inactivated by incubating at 75ºC for 10 min. The samples were then further treated with 0.1 mg/mL Proteinase K (Invitrogen) and 0.5% SDS and were incubated at 55ºC for 1 h. Samples were then extracted once with phenol-chloroform: isoamyl alcohol (25:24:1) and a second time with chloroform. DNA was isolated by ethanol precipitation with the addition of 0.3 M sodium acetate. DNA quality and quantity were determined using a NanoDrop spectrophotometer (Thermo Fischer Scientific).

For measuring phage genome abundance, 25 µL reactions consisted of 5 µL each 0.625 µM primers 1 and 2, 12.5 µL 2X SYBR master mix, and 2.5 µL of 2.5 ng/µL phage genomic DNA. qPCR reactions were performed in technical duplicates for biological triplicate samples. The relative abundance was calculated by comparing the C_t values of phage infected *E. coli* with AvcID to inactive AvcID* at each timepoints.

Alkylation of T7 phage

Alkylation of T7 phage was performed as previously described with slight modifications [31]. Phage lysates were treated for 2 hr at 37°C either with 0.01 M methyl methanesulfonate (MMS) (Santa Cruz Biotechnology) or equal volume of phage buffer (100 µM Tris pH 7.5, 10 mM $MgSO_4$, and 36 mM $CaCl_2$). The treated phage was then chilled on ice for 10 minutes and then dialyzed overnight at 4°C against phage buffer with 10 kDA dialysis tube (Thermo Scientific). Phage titers after alkylation and dialysis were determined using the small-drop plaque assay.

Transmission Electron Microscopy (TEM)

High titer phage stocks were prepared using a 15 mL soft agar overlay with 150 µL of *E. coli* DH10B and 150 µL of $2.26x10^{10}$ PFU/mL (T5 or T7). Liquid cultures were then grown using 30 mL LB with 100 µL plus 0.5 mL overnight culture harboring a plasmid with active or inactive *avcID* system (AmpR) and one plaque (either T5 or T7). The culture was grown at RT while shaking at 200 RPM for 6 hours or until clear. 3mL of chloroform was added and the culture was incubated for an additional 5 minutes before being centrifuged at 8,000 x g (~7,000 RPM in F14-14x50cy rotor) for 10 minutes at 4°C. The supernatant was then spun at 26,000 x g (~12,500 RPM in F14-14x50cy rotor) for 90 minutes at 4°C to pellet the phage. The pellet was resuspended in 1.5 mL of phage buffer (10 mM Tris, pH 7.6, 10mM $MgCl_2$) by nutating overnight at 4°C.

Approximately ~5 µL of phage samples were applied to freshly glow discharged (PELCO easiGlow, 15 mA, 45 s) continuous carbon support film grids (Ted Pella, Cat. No: 1754-F) for 60 seconds, followed by washing with distilled water and then staining with 1% aqueous Uranyl Acetate (Electron Microscopy Solutions, Cat. No: 22400-4). Grids were blotted dry with Whatman filter paper. The phage samples were imaged at the RTSF Cryo-EM Core Facility at Michigan State University using a Talos Arctica operated at 200 keV. Micrographs were

collected on a Ceta camera at a nominal magnification of 45,000 (2.2 Å/pixel) and 57,000 (1.8 Å/pixel) with an exposure time of 1 second and objective lens defocus setting of 5 µM underfocus.

Statistical Analysis

As specified in the figure legends, all of the statistical analyses were analyzed in GraphPad Prism Software. Statistical significances are denoted as follows: a single asterisk (*) indicates $p < 0.05$; double asterisks (**) indicate $p < 0.01$; triple asterisks (***) indicate $p < 0.001$; and quadruple asterisks (****) indicate $p < 0.0001$. Means ± SEM and specific n values are reported in each figure legend.

REFERENCE

1. Makarova KS, Wolf YI, Snir S, Koonin E V. 2011. Defense Islands in Bacterial and Archaeal Genomes and Prediction of Novel Defense Systems. J Bacteriol 193:6039–6056.
2. Enikeeva FN, Severinov K V., Gelfand MS. 2010. Restriction-modification systems and bacteriophage invasion: who wins? J Theor Biol 266:550.
3. Cohen D, Melamed S, Millman A, Shulman G, Oppenheimer-Shaanan Y, Kacen A, Doron S, Amitai G, Sorek R. 2019. Cyclic GMP–AMP signalling protects bacteria against viral infection. Nature 574:691–695.
4. Millman A, Bernheim A, Stokar-Avihail A, Fedorenko T, Voichek M, Leavitt A, Oppenheimer-Shaanan Y, Sorek R. 2020. Bacterial Retrons Function In Anti-Phage Defense. Cell 183:1551-1561.e12.
5. Page R, Peti W. 2016. Toxin-antitoxin systems in bacterial growth arrest and persistence. Nat Chem Biol 2016 124 12:208–214.
6. Bernheim A, Sorek R. 2020. The pan-immune system of bacteria: antiviral defence as a

community resource. Nat Rev Microbiol 18:113–119.

7. Doron S, Melamed S, Ofir G, Leavitt A, Lopatina A, Keren M, Amitai G, Sorek R. 2018. Systematic discovery of antiphage defense systems in the microbial pangenome. Science (80-) 359:eaar4120.

8. Ogura T, Hiraga S. 1983. Mini-F plasmid genes that couple host cell division to plasmid proliferation. Proc Natl Acad Sci 80:4784–4788.

9. Gotfredsen M, Gerdes K. 1998. The *Escherichia coli* relBE genes belong to a new toxin–antitoxin gene family. Mol Microbiol 29:1065–1076.

10. Lehnherr H, Maguin E, Jafri S, Yarmolinsky MB. 1993. Plasmid addiction genes of bacteriophage P1: doc, which causes cell death on curing of prophage, and phd, which prevents host death when prophage is retained. J Mol Biol 233:414–28.

11. Harms A, Brodersen DE, Mitarai N, Gerdes K. 2018. Toxins, Targets, and Triggers: An Overview of Toxin-Antitoxin Biology. Mol Cell 70:768–784.

12. Guglielmini J, Van Melderen L. 2011. Bacterial toxin-antitoxin systems: Translation inhibitors everywhere. Mob Genet Elements 1:283–290.

13. Song S, Wood TK. 2020. A Primary Physiological Role of Toxin/Antitoxin Systems Is Phage Inhibition. Front Microbiol 11:1895.

14. Choi JS, Kim W, Suk S, Park H, Bak G, Yoon J, Lee Y. 2018. The small RNA, SdsR, acts as a novel type of toxin in *Escherichia coli*. RNA Biol 15:1319–1335.

15. Peltier J, Hamiot A, Garneau JR, Boudry P, Maikova A, Hajnsdorf E, Fortier L-C, Dupuy B, Soutourina O. 2020. Type I toxin-antitoxin systems contribute to the maintenance of mobile genetic elements in *Clostridioides difficile*. Commun Biol 3:718.

16. LeRoux M, Culviner PH, Liu YJ, Littlehale ML, Laub MT. 2020. Stress Can Induce Transcription of Toxin-Antitoxin Systems without Activating Toxin. Mol Cell 79:280-292.e8.

17. Pecota DC, Wood TK. 1996. Exclusion of T4 phage by the hok/sok killer locus from

642 plasmid R1. J Bacteriol 178:2044–2050.
643 18. Hazan R, Engelberg-Kulka H. 2004. *Escherichia coli* mazEF-mediated cell death as a
644 defense mechanism that inhibits the spread of phage P1. Mol Genet Genomics 272:227–
645 234.
646 19. Guegler CK, Laub MT. 2021. Shutoff of host transcription triggers a toxin-antitoxin system
647 to cleave phage RNA and abort infection. Mol Cell 81:2361-2373.e9.
648 20. Dy RL, Przybilski R, Semeijn K, Salmond GPCC, Fineran PC. 2014. A widespread
649 bacteriophage abortive infection system functions through a Type IV toxin-antitoxin
650 mechanism. Nucleic Acids Res 42:4590–605.
651 21. Szekeres S, Dauti M, Wilde C, Mazel D, Rowe-Magnus DA. 2007. Chromosomal toxin-
652 antitoxin loci can diminish large-scale genome reductions in the absence of selection. Mol
653 Microbiol 63:1588–605.
654 22. Pandey DP, Gerdes K. 2005. Toxin-antitoxin loci are highly abundant in free-living but
655 lost from host-associated prokaryotes. Nucleic Acids Res 33:966–976.
656 23. Hsueh BY, Severin GB, Elg CA, Waldron EJ, Kant A, Wessel AJ, Dover JA, Rhoades CR,
657 Ridenhour BJ, Parent KN, Neiditch MB, Ravi J, Top EM, Waters CM. 2022. Phage
658 defence by deaminase-mediated depletion of deoxynucleotides in bacteria. Nat Microbiol
659 7:1210–1220.
660 24. Tal N, Millman A, Stokar-Avihail A, Fedorenko T, Leavitt A, Melamed S, Yirmiya E,
661 Avraham C, Brandis A, Mehlman T, Amitai G, Sorek R. 2022. Bacteria deplete
662 deoxynucleotides to defend against bacteriophage infection. Nat Microbiol 7:1200–1209.
663 25. Berdygulova Z, Esyunina D, Miropolskaya N, Mukhamedyarov D, Kuznedelov K, Nickels
664 BE, Severinov K, Kulbachinskiy A, Minakhin L. 2012. A novel phage-encoded
665 transcription antiterminator acts by suppressing bacterial RNA polymerase pausing.
666 Nucleic Acids Res 40:4052.
667 26. You L, Shi J, Shen L, Li L, Fang C, Yu C, Cheng W, Feng Y, Zhang Y. 2019. Structural

basis for transcription antitermination at bacterial intrinsic terminator. Nat Commun 2019 101 10:1–11.

27. Hesselbach BA, Nakada D. 1977. “Host shutoff” function of bacteriophage T7: involvement of T7 gene 2 and gene 0.7 in the inactivation of *Escherichia coli* RNA polymerase. J Virol 24:736–45.

28. Davison J. 2015. Pre-early functions of bacteriophage T5 and its relatives. Bacteriophage 5:e1086500.

29. Lindahl T, Ljungquist S, Siegert W, Nyberg B, Sperens B. 1977. DNA N-glycosidases: properties of uracil-DNA glycosidase from *Escherichia coli*. J Biol Chem 252:3286–94.

30. Lindahl T. 1990. Repair of intrinsic DNA lesions. Mutat Res 238:305–11.

31. Czaika G, Mamet-Bratley MD, Karska-Wysocki B. 1986. Mechanism of inhibition of bacteriophage T7 DNA synthesis in *Escherichia coli* B cells infected by alkylated bacteriophage T7. Mutat Res Repair Reports 166:1–8.

32. Tock MR, Dryden DTF. 2005. The biology of restriction and anti-restriction. Curr Opin Microbiol 8:466–72.

33. Dussoix D, Arber W. 1962. Host specificity of DNA produced by *Escherichia coli*. II. Control over acceptance of DNA from infecting phage lambda. J Mol Biol 5:37–49.

34. Lowey B, Whiteley AT, Keszei AFA, Morehouse BR, Mathews IT, Antine SP, Cabrera VJ, Kashin D, Niemann P, Jain M, Schwede F, Mekalanos JJ, Shao S, Lee ASY, Kranzusch PJ. 2020. CBASS Immunity Uses CARF-Related Effectors to Sense 3′–5′- and 2′–5′-Linked Cyclic Oligonucleotide Signals and Protect Bacteria from Phage Infection. Cell 182:38-49.e17.

35. Bernheim A, Millman A, Ofir G, Meitav G, Avraham C, Shomar H, Rosenberg MM, Tal N, Melamed S, Amitai G, Sorek R. 2020. Prokaryotic viperins produce diverse antiviral molecules. Nature https://doi.org/10.1038/s41586-020-2762-2.

36. LeRoux M, Srikant S, Teodoro GIC, Zhang T, Littlehale ML, Doron S, Badiee M, Leung

AKL, Sorek R, Laub MT. 2022. The DarTG toxin-antitoxin system provides phage defence by ADP-ribosylating viral DNA. Nat Microbiol 7:1028–1040.

37. Hinton DM. 2010. Transcriptional control in the prereplicative phase of T4 development. Virol J 7:289.

38. Short FL, Akusobi C, Broadhurst WR, Salmond GPC. 2018. The bacterial Type III toxin-antitoxin system, ToxIN, is a dynamic protein-RNA complex with stability-dependent antiviral abortive infection activity. Sci Rep 8:1013.

39. Brantl S, Jahn N. 2015. sRNAs in bacterial type I and type III toxin-antitoxin systems. FEMS Microbiol Rev 39:413–427.

40. Goeders N, Chai R, Chen B, Day A, Salmond GPC. 2016. Structure, Evolution, and Functions of Bacterial Type III Toxin-Antitoxin Systems. Toxins (Basel) 8.

41. Kasman LM, Porter LD. 2022. BacteriophagesStatPearls. StatPearls Publishing. https://www.ncbi.nlm.nih.gov/books/NBK493185/. Retrieved 3 September 2022.

42. Birch EW, Ruggero NA, Covert MW. 2012. Determining host metabolic limitations on viral replication via integrated modeling and experimental perturbation. PLoS Comput Biol 8:e1002746.

43. Mahata T, Molshanski-Mor S, Goren MG, Jana B, Kohen-Manor M, Yosef I, Avram O, Pupko T, Salomon D, Qimron U. 2021. A phage mechanism for selective nicking of dUMP-containing DNA. Proc Natl Acad Sci U S A 118.

44. Liao Y-T, Liu F, Wu VCH. 2019. Complete Genome Sequence of a Lytic T7-Like Phage, *Escherichia* Phage vB_EcoP-Ro45lw, Isolated from Nonfecal Compost Samples. Microbiol Resour Announc 8.

45. Boeckman J, Korn A, Yao G, Ravindran A, Gonzalez C, Gill J. 2022. Sheep in wolves' clothing: Temperate T7-like bacteriophages and the origins of the Autographiviridae. Virology 568:86–100.

46. Weigele P, Raleigh EA. 2016. Biosynthesis and Function of Modified Bases in Bacteria

and Their Viruses. Chem Rev 116:12655–12687.

47. Endy D, You L, Yin J, Molineux IJ. 2000. Computation, prediction, and experimental tests of fitness for bacteriophage T7 mutants with permuted genomes. Proc Natl Acad Sci U S A 97:5375–5380.

48. O'Hara BJ, Alam M, Ng W-L. 2022. The *Vibrio cholerae* Seventh Pandemic Islands act in tandem to defend against a circulating phage. PLoS Genet 18:e1010250.

49. Bose JL, Rosenberg CS, Stabb E V. 2008. Effects of luxCDABEG induction in *Vibrio fischeri*: Enhancement of symbiotic colonization and conditional attenuation of growth in culture. Arch Microbiol 190:169–183.

50. Mazzocco A, Waddell TE, Lingohr E, Johnson RP. 2009. Enumeration of bacteriophages using the small drop plaque assay system. Methods Mol Biol 501:81–85.

51. Fernandez NL, Waters CM. 2019. Cyclic di-GMP Increases Catalase Production and Hydrogen Peroxide Tolerance in *Vibrio cholerae*. Appl Environ Microbiol 85.

52. Kao C, Rüdisser S, Zheng M. 2001. A simple and efficient method to transcribe RNAs with reduced 3' heterogeneity. Methods 23:201–5.

53. Schindelin J, Arganda-Carreras I, Frise E, Kaynig V, Longair M, Pietzsch T, Preibisch S, Rueden C, Saalfeld S, Schmid B, Tinevez J-Y, White DJ, Hartenstein V, Eliceiri K, Tomancak P, Cardona A. 2012. Fiji: an open-source platform for biological-image analysis. Nat Methods 9:676–682.

54. Fernandez NL, Hsueh BY, Nhu NTQ, Franklin JL, Dufour YS, Waters CM. 2020. *Vibrio cholerae* adapts to sessile and motile lifestyles by cyclic di-GMP regulation of cell shape. Proc Natl Acad Sci 117:29046–29054.

55. Dover JA, Burmeister AR, Molineux IJ, Parent KN. 2016. Evolved populations of *Shigella flexneri* phage Sf6 acquire large deletions, altered genomic architecture, and faster life cycles. Genome Biol Evol 8:2827–2840.

Figure Legends

Figure 1: The AvcID system provides phage defense in liquid culture.

Growth curves for *E. coli* with active (pAvcID) or inactive (pAvcID*) after infection with T5 (**A**) or T7 (**B**) phage at varying multiplicities of infection (MOI). Data represents the mean ± SEM of three biological replicate cultures.

Figure 2: Transcriptional shutoff leads to the degradation of *avcI*.

Shown are Northern blots of *avcI* RNA using a biotinylated probe complementary to *avcI* (top) and Western blots of AvcD-6xHis using anti-6xHis antibody (bottom) during rifampicin treatment (250 µg/mL) (**A**), spectinomycin treatment (200 µg/mL) (**B**), T5 infection (**C**), and T7 infection (**D**) at a MOI of 5.

Figure 3: AvcD is activated by T5 and T7 phages.

In vivo abundance of dCTP (**A**) and dCMP (**B**) in an *E. coli* host carrying pAvcID or pAvcID* with its native promoter before and after infection of T5 (MOI = 5) or T7 phage (MOI = 5). Nucleotides were measured using UPLC-MS/MS and normalized to total protein. Data represents the mean ± SEM of three biological replicate cultures, Two-way ANOVA with Dunnett's post-hoc test, and ns indicates not significant.

Figure 4: AvcID reduces the functionality of T5 but not T7 phage.

Survival of *E. coli* encoding the indicated AvcID systems as measured by CFU after infection with T5 (**A**) or T7 (**D**). PFU quantification over time in cultures of pAvcID or pAvcID* containing cells infected with T5 (**B**) or T7 (**E**). Relative T5 (**C**) or T7 (**F**) genome abundance comparing *E. coli* expressing pAvcID or inactive AvcID* over time. Percent viable phage after infecting cells

containing AvcID with T5 or T7 phages (**G**). Data represents the mean ± SEM of three biological replicate cultures.

Figure 5: TEM of AvcID-induced Phage Defense. Transmission Electron Microscopy (TEM) of T5 (**A, B**) or T7 (**C**) from *E. coli* host carrying pAvcID (**A**, **C**) or pAvcID* (**B**). Samples were negative stained with 1% (w/v) uranyl acetate. Scale bar 100 nm. All samples were analyzed in three biological replicates with similar results.

Figure 6: Ung and AvcID do not function together to provide phage protection. (**A**) Growth curves for *E. coli* MG1655 or Δ*ung* mutant with pAvcID or pAvcID* after infection with T5 phage at varying multiplicities of infection (MOI). Data represents the mean ± SEM of three biological replicate cultures. (**B**) Measurement of phage titer on WT *E. coli* MG1655 or Δ*ung E. coli* encoding either active or inactive AvcID system infected with T5 phage. Data represents the mean ± SEM of three biological replicate cultures. (**C**) Measurement of phage titer on WT *E. coli* MG1655 co-expressing Dut and either active or inactive AvcID system infected by T5 phage. Data represents the mean ± SEM of three biological replicate cultures.

Figure 7: AvcID reduces the functionality of $T7^{412}$ mutant phage. Representative images of tenfold serial dilution plaque assays of $T7^{WT}$ (**A**) or $T7^{412}$ (**B**) phages spotted on *E. coli* MG1655 expressing either active (top) or inactive (bottom) *avcID* system. Images are representative of three replicates. (**C**) CFU quantification of *E. coli* MG1655 over time in cultures indicated AvcID systems after infection with mutant $T7^{412}$. (**D**) PFU quantification over time in cultures of indicated AvcID systems-containing cells infected with $T7^{412}$. (**E**) Relative $T7^{412}$ genome abundance comparing *E. coli* expressing pAvcID or

796 inactive AvcID* over time. (**F**) Percent viable phage after infecting cells containing AvcID with
797 $T7^{412}$. Data represents the mean ± SEM of three biological replicate cultures.
798
799 **Figure 8: Relationship between phage lysis time versus protection conferred by AvcID.**
800 The phage lysis time is determined as the time at the initial drop in OD_{600} by phage at MOI of 1
801 while the amount of protection conferred by AvcID is determined by taking the difference of the
802 area under the growth curves between cells containing active or inactive AvcID at MOI of 0.01.
803 Circles indicate the phages belong to the *Myoviridae* family; triangle belongs to the *Podoviridae*
804 family; square indicates *Siphoviridae* family; and diamond indicates *Microviridae* family.

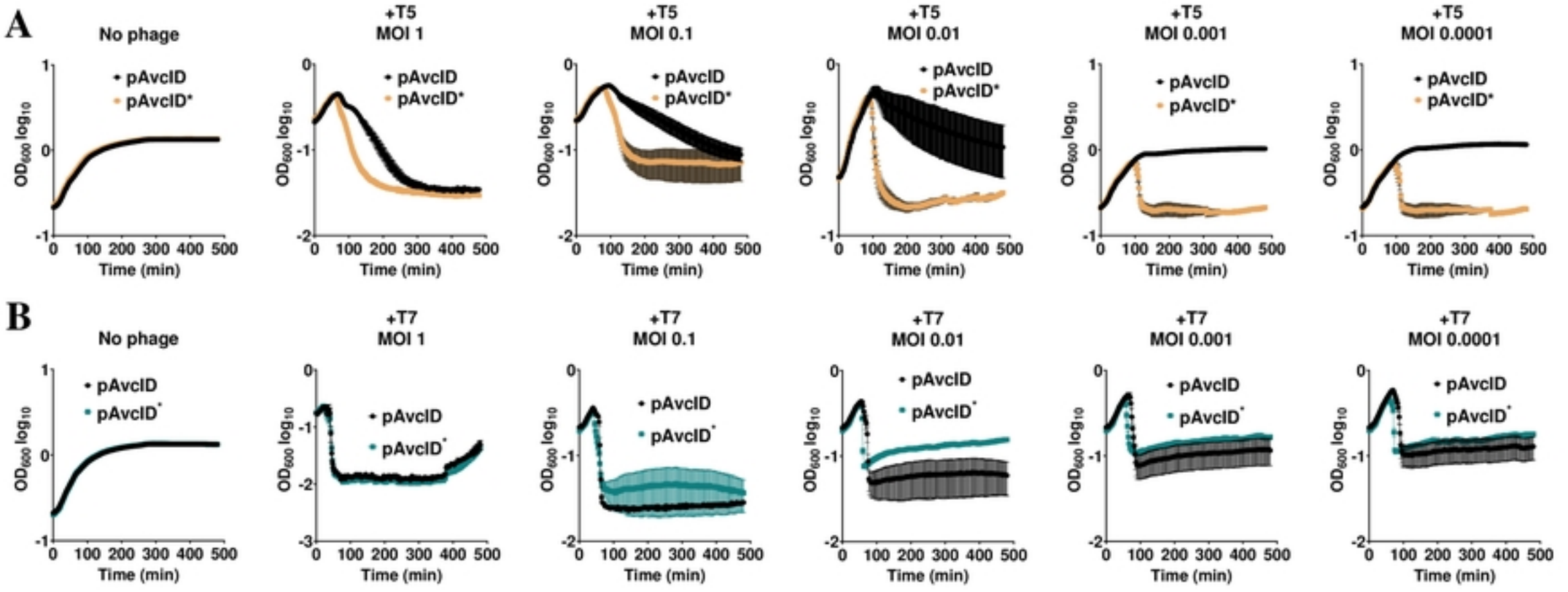

Figure 1: The AvcID system provides phage defense in liquid culture.
Growth curves for *E. coli* with active (pAvcID) or inactive (pAvcID*) after infection with T5 (A) or T7 (B) phage at varying multiplicities of infection (MOI). Data represents the mean ± SEM of three biological replicate cultures.

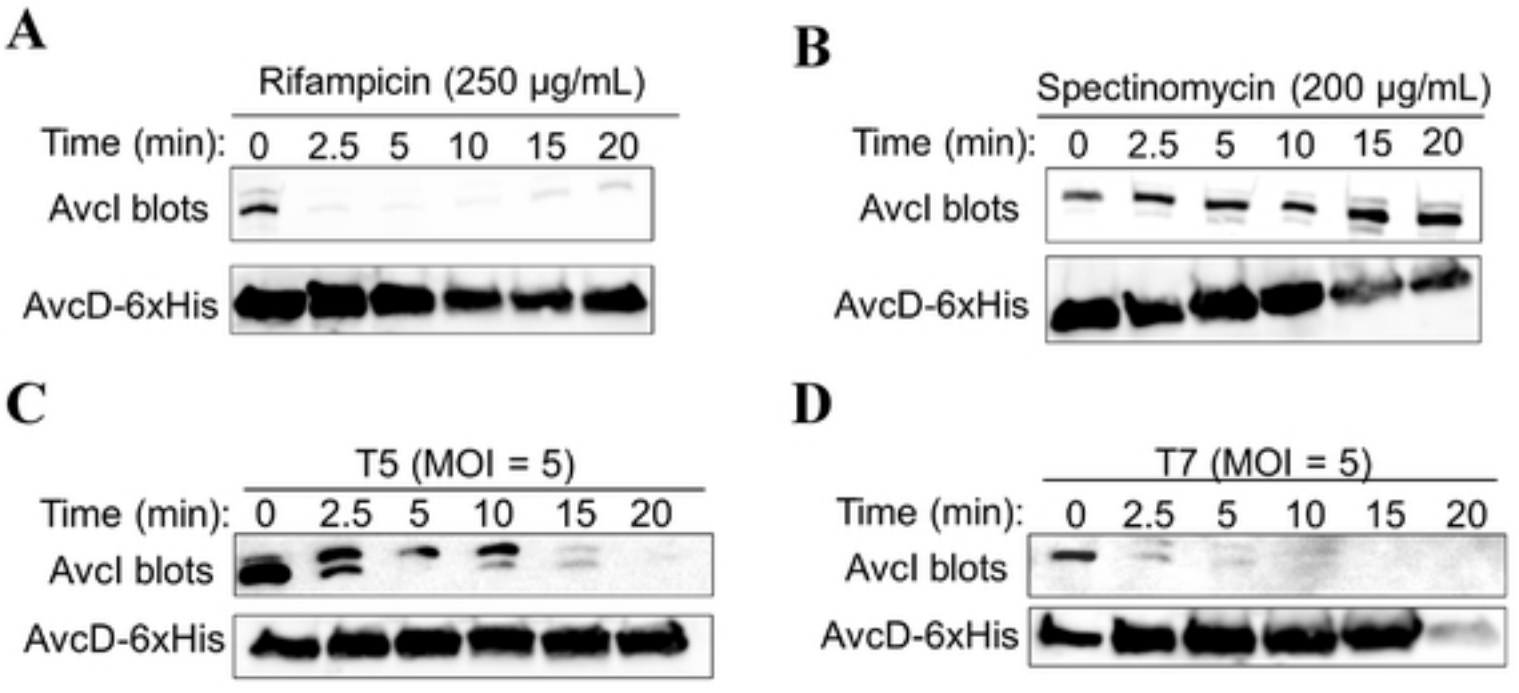

Figure 2: Transcriptional shutoff leads to the degradation of avcI.
Shown are Northern blots of *avcI* RNA using a biotinylated probe complementary to AvcI (top) and Western blots of AvcD-6xHis using anti-6xHis antibody (bottom) during rifampicin treatment (250 µg/mL) (A), spectinomycin treatment (200 µg/mL) (B), T5 infection (C), and T7 infection (D) at a MOI of 5.

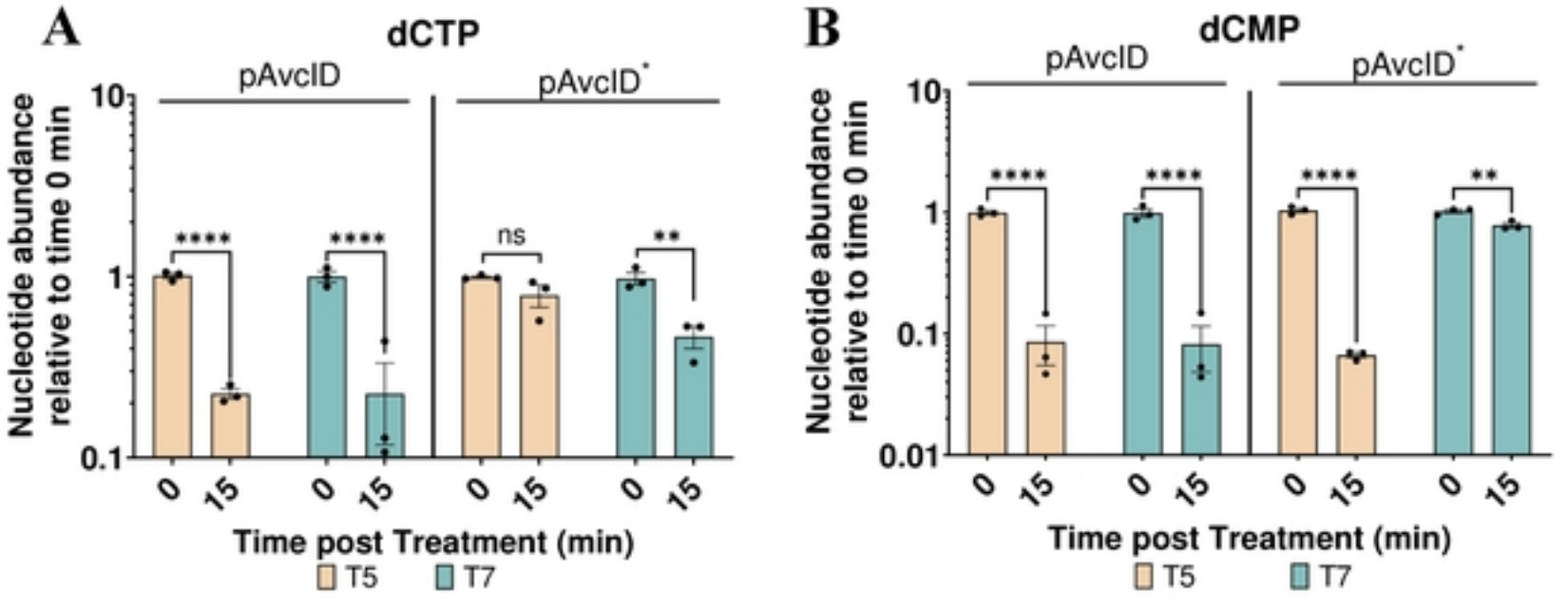

Figure 3: AvcD is activated by T5 and T7 phages.
In vivo abundance of dCTP (A) and dCMP (B) in an E. coli host carrying pAvcID or pAvcID* with its native promoter before and after infection of T5 (MOI = 5) or T7 phage (MOI = 5). Nucleotides were measured using UPLC-MS/MS and normalized to total protein. Data represents the mean ± SEM of three biological replicate cultures, Two-way ANOVA with Dunnett's post-hoc test, and ns indicates not significant.

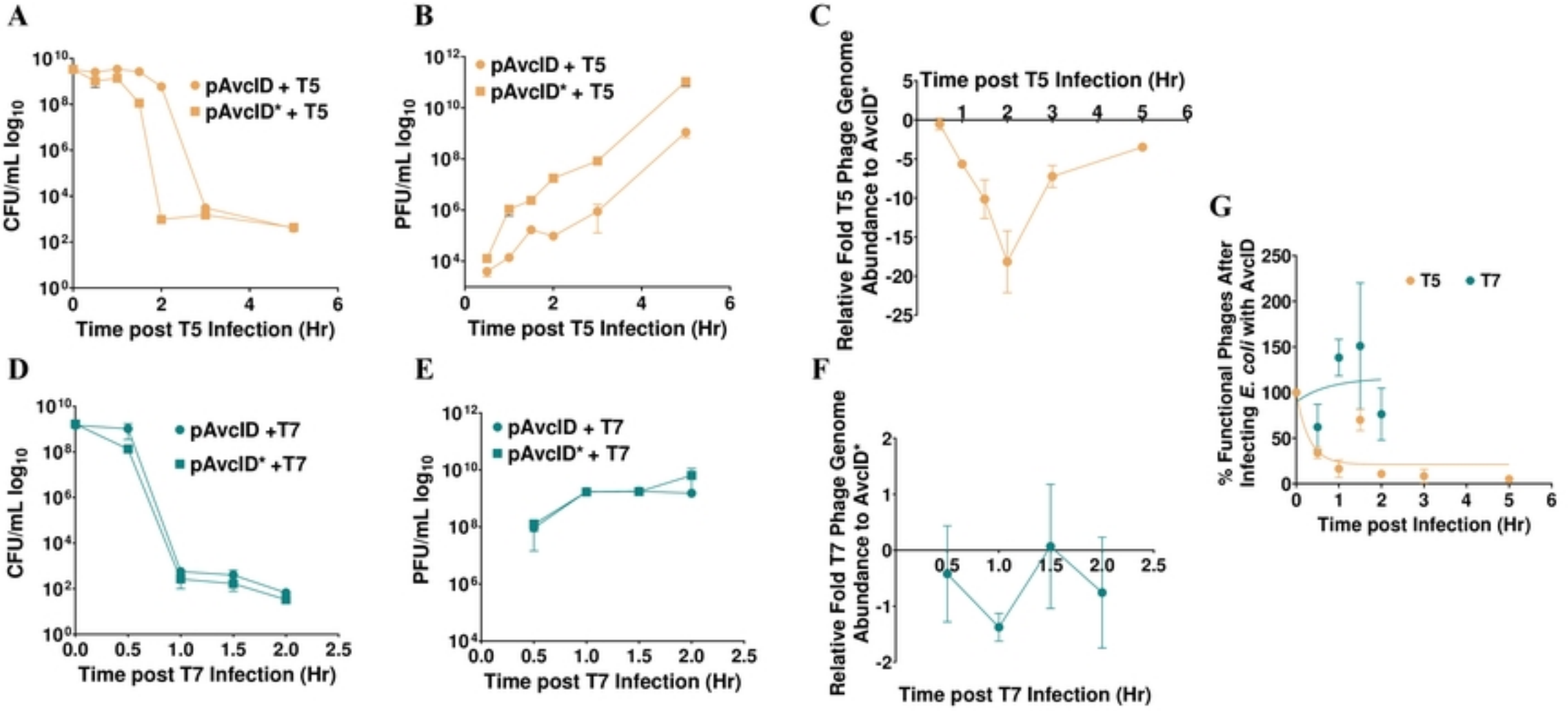

Figure 4: AvcID reduces the functionality of T5 but not T7 phage.

Survival of E. coli encoding the indicated AvcID systems as measured by CFU after infection with T5 (A) or T7 (D). PFU quantification over time in cultures of pAvcID or pAvcID* containing cells infected with T5 (B) or T7 (E). Relative T5 (C) or T7 (F) genome abundance comparing E. coli expressing pAvcID or inactive AvcID* over time. Percent viable phage after infecting cells containing AvcID with T5 or T7 phages (G). Data represents the mean ± SEM of three biological replicate cultures.

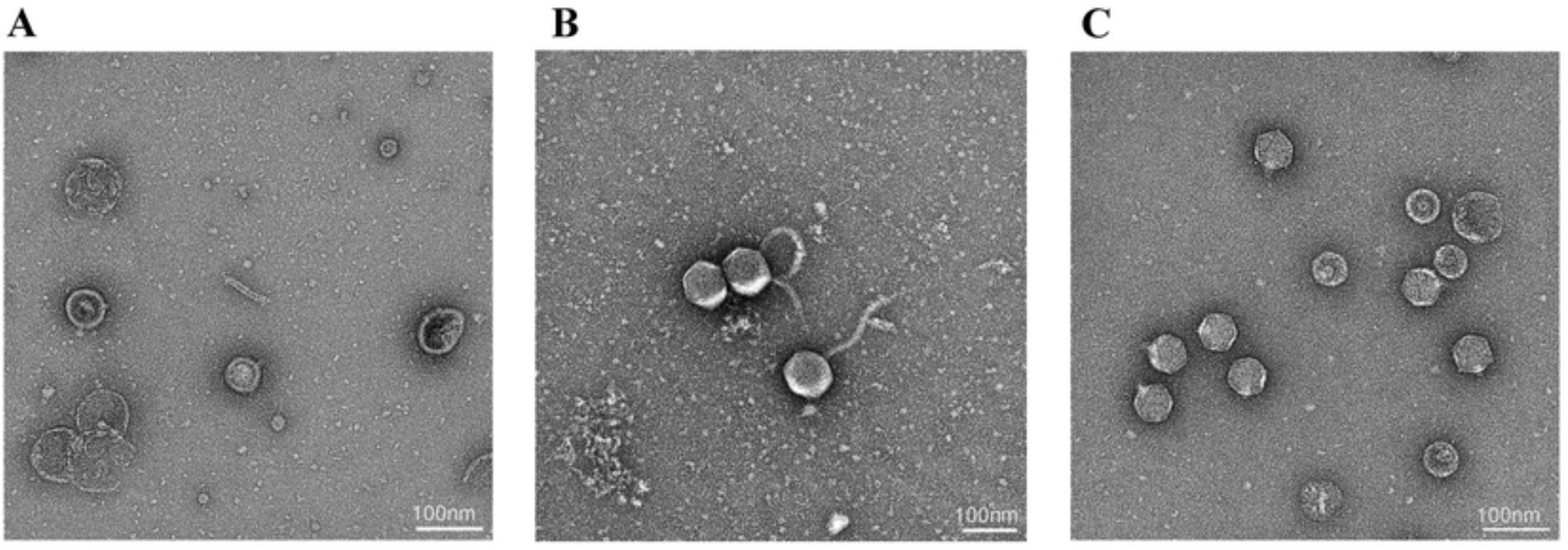

Figure 5: TEM of AvcID-induced Phage Defense. Transmission Electron Microscopy (TEM) of T5 (A, B) or T7 (C) from E. coli host carrying pAvcID (A, C) or pAvcID* (B). Samples were negative stained with 1% (w/v) uranyl acetate. Scale bar 100 nm. All samples were analyzed in three biological replicates with similar results.

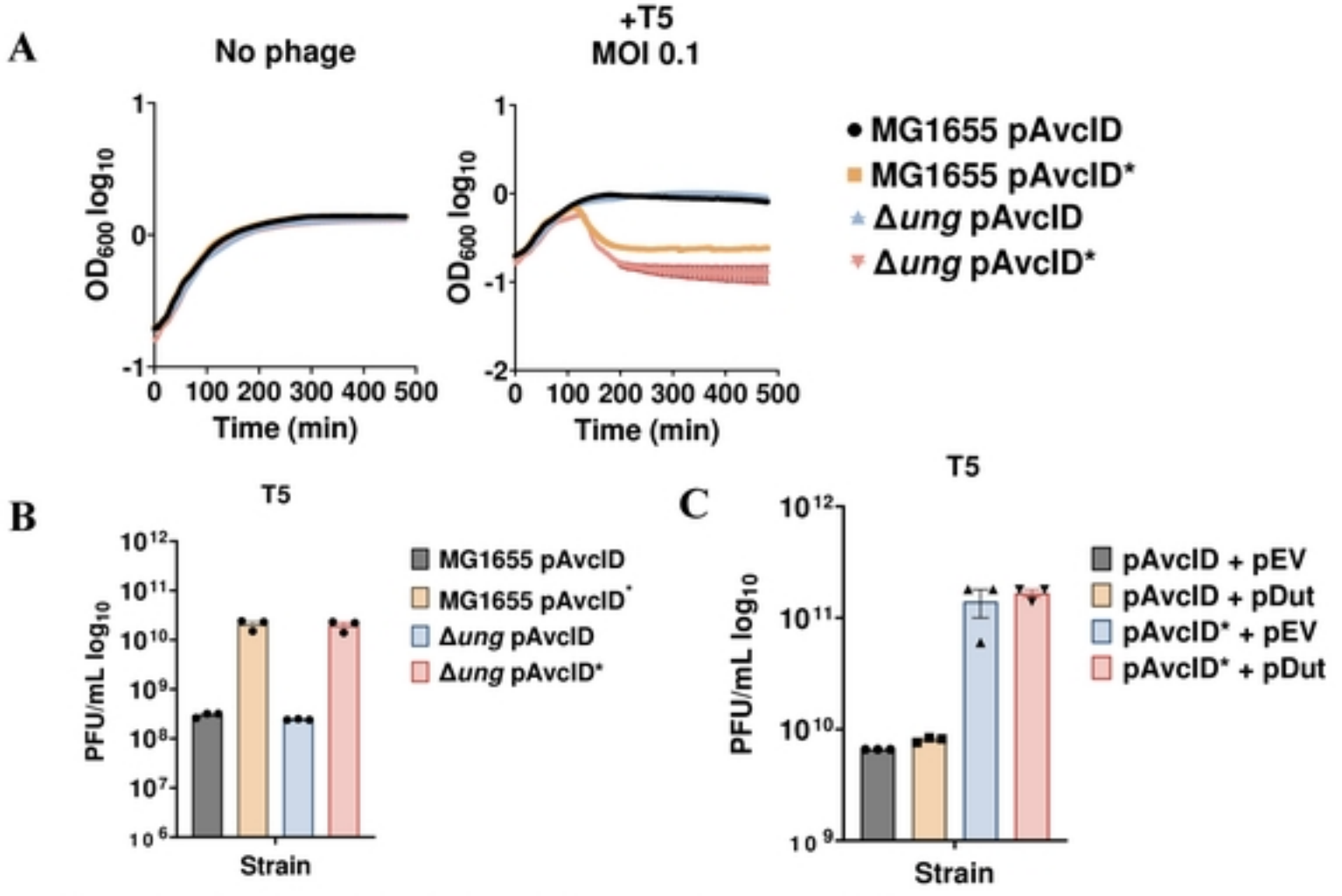

Figure 6: Ung and AvcID do not function together to provide phage protection.
(A) Growth curves for *E. coli* MG1655 or Δ*ung* mutant with pAvcID or pAvcID* after infection with T5 phage at varying multiplicities of infection (MOI). Data represents the mean ± SEM of three biological replicate cultures. (B) Measurement of phage titer on WT *E. coli* MG1655 or Δ*ung E. coli* encoding either active or inactive AvcID system infected with T5 phage. Data represents the mean ± SEM of three biological replicate cultures. (C) Measurement of phage titer on WT *E. coli* MG1655 co-expressing Dut and either active or inactive AvcID system infected by T5 phage. Data represents the mean ± SEM of three biological replicate cultures.

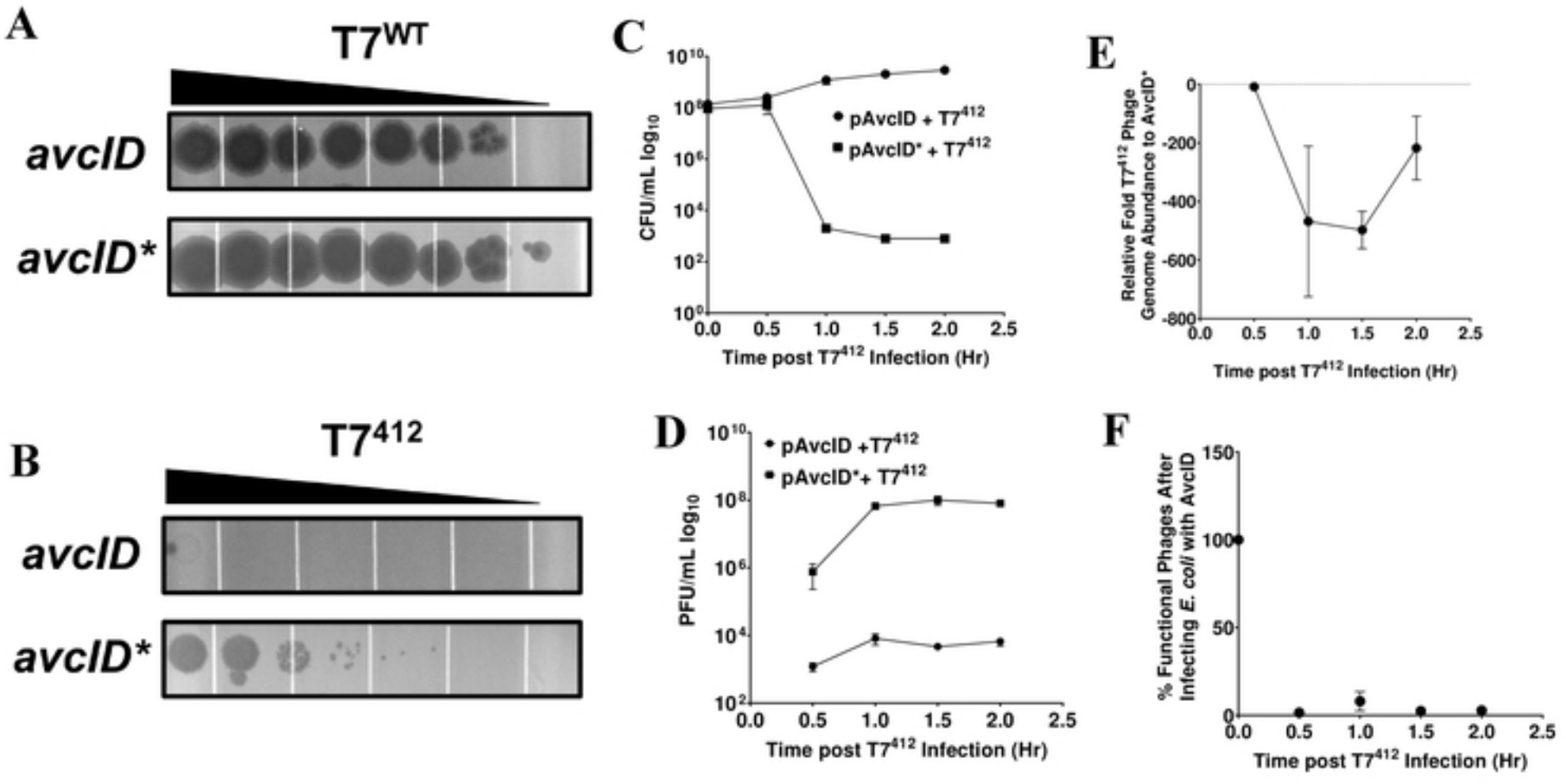

Figure 7: AvcID reduces the functionality of $T7^{412}$ mutant phage.
Representative images of tenfold serial dilution plaque assays of $T7^{WT}$ (A) or $T7^{412}$ (B) phages spotted on *E. coli* MG1655 expressing either active (top) or inactive (bottom) avcID system. Images are representative of three replicates. (C) CFU quantification of *E. coli* MG1655 over time in cultures indicated AvcID systems after infection with mutant $T7^{412}$. (D) PFU quantification over time in cultures of indicated AvcID systems-containing cells infected with $T7^{412}$. (E) Relative $T7^{412}$ genome abundance comparing *E. coli* expressing pAvcID or inactive AvcID* over time. (F) Percent viable phage after infecting cells containing AvcID with $T7^{412}$. Data represents the mean ± SEM of three biological replicate cultures.

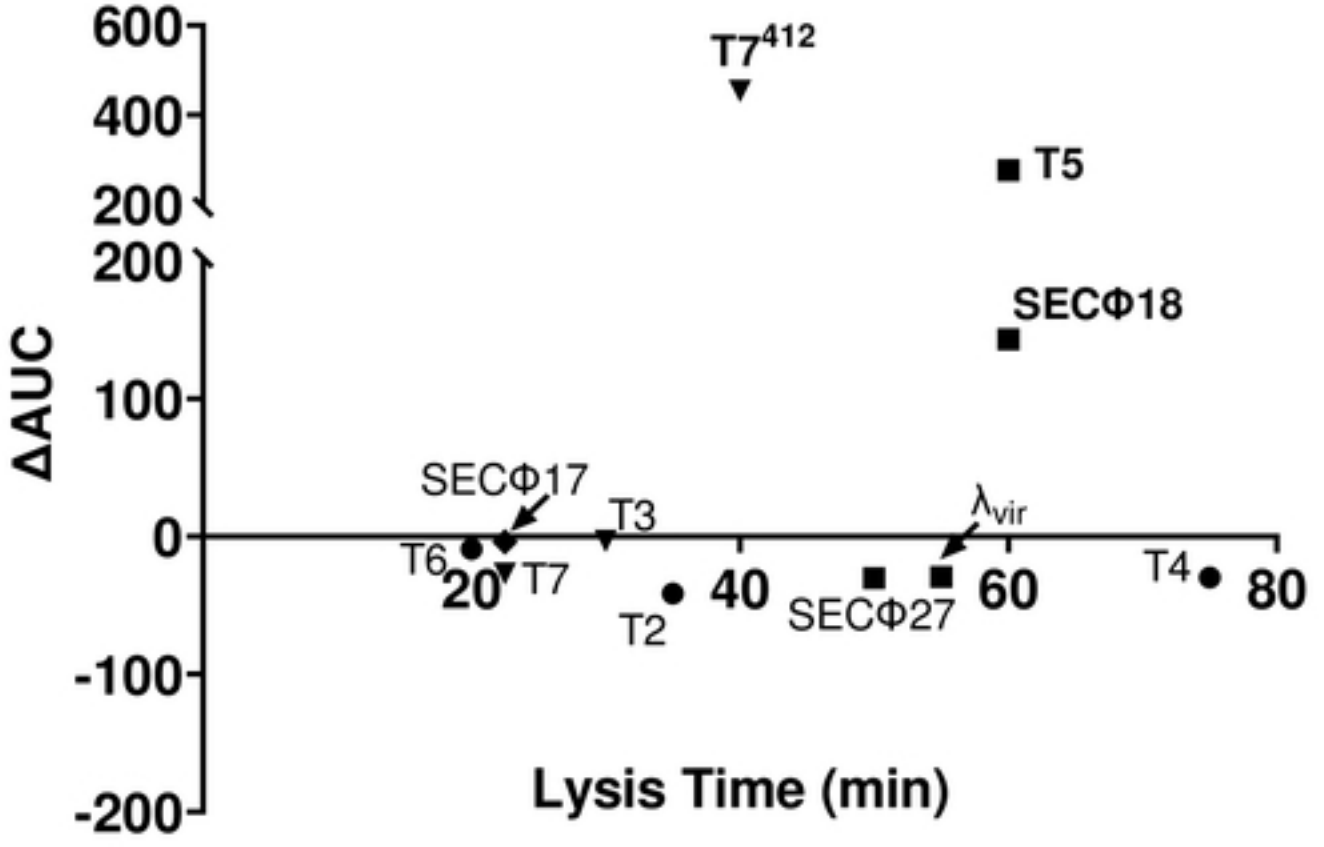

Figure 8: Relationship between phage lysis time versus protection conferred by AvcID.
The phage lysis time is determined as the time at the initial drop in OD_{600} by phage at MOI of 1 while the amount of protection conferred by AvcID is determined by taking the difference of the area under the growth curves between cells containing active or inactive AvcID at MOI of 0.01. Circles indicate the phages belong to the *Myoviridae* family; triangle belongs to the *Podoviridae* family; square indicates *Siphoviridae* family; and diamond indicates *Microviridae* family.